Journal of Applied Mathematics and Computational Mechanics 2026, 25(3), 82-99
www.amcm.pcz.pl p-ISSN 2299-9965
DOI: 10.17512/jamcm.2026.3.06 e-ISSN 2353-0588

BIOMECHANICAL ANALYSIS OF THE EFFECTS OF SPRING-ASSISTED CRANIAL DISTRACTION IN CHILDREN IN CRITICAL PHASES OF DEVELOPMENT

***Arkadiusz Szarek*[1]*, Piotr Paszta*[1,*]*, Dawid Larysz*[2, 3]*, Patrycja Larysz*[2, 3]**

[1] *Faculty of Mechanical Engineering, Czestochowa University of Technology*
Częstochowa, Poland
[2] *Department of Head and Neck Surgery for Children and Adolescents*
Prof. St. Popowski Regional Specialized Children's Hospital
Olsztyn, Poland
[3] *Department of Head and Neck Surgery for Children and Adolescents*
University of Warmia and Mazury
Olsztyn, Poland
arkadiusz.szarek@pcz.pl, piotr.paszta@pcz.pl, dawid.larysz@uwm.edu.pl
patrycja.larysz@wssd.olsztyn.pl

Received: 13 June 2026; Accepted: 8 September 2026

Abstract. The aim of the study was a numerical biomechanical analysis of the effects of spring-assisted distraction in children with sagittal craniosynostosis in critical phases of development. Three-dimensional skull models of infants aged 3, 6, and 12 months, generated based on computed tomography data, were examined. The loads generated by springs with forces of 4.8 N, 8 N, and 13.2 N were simulated in the ANSYS environment. The analysis incorporated physiological intracranial pressure as well as changes in the stiffness of bones and cranial sutures that progress with age. The obtained results indicate that the skulls of 3-month-old infants undergo significant deformations that substantially exceed safety limits for all tested forces. In the case of 6-month-old children, the load of 4.8 N is at the safety limit. Conversely, in 12-month-old patients, despite a safe level of deformation, dangerous stress concentrations were observed directly at the points of contact between the springs and the bone tissue. The conducted research proves that the treatment requires the application of fully personalized methods and a highly precise selection of the distraction force tailored to the individual biomechanics of each patient.

MSC 2010: *92C10*
Keywords: *biomechanics, craniosynostosis, FEM, spring-assisted distraction, ANSYS*

---

[*] Corresponding author

1. Introduction

The research is conducted with the approval of the Bioethics Committee for Scientific Research at the Jerzy Kukuczka Academy of Physical Education in Katowice, dated June 5, 2025 – Resolution No. 10-VI/2025.

The advancement of computational systems, breakthroughs in biomaterials, and a deeper understanding of the molecular biology of developmental anomalies mark a turning point that is fundamentally reshaping traditional surgical techniques in pediatric craniofacial surgery [1-3].

Cranial sutures play a pivotal role as sites of intramembranous bone growth, which is essential for proper cranial development. Craniosynostosis is a congenital defect characterized by the premature fusion of these sutures, necessitating the application of evidence-based practices in modern medicine. A prevalent issue is the non-syndromic form of this condition, particularly the frequently encountered isolated sagittal synostosis. This condition not only leads to a visible deformation of the cranial shape but also poses severe neurological risks. Research indicates that the medical literature frequently underestimates the true incidence of dangerously elevated intracranial pressure in patients awaiting surgery. Consequently, precise preoperative diagnostics and timely surgical intervention are critical for cerebral decompression. Today, the planning of such reconstructive surgeries is becoming increasingly precise due to an interdisciplinary approach and biomedical engineering. To achieve this, researchers are developing advanced, population-specific material and biomechanical models of the skull. These tools facilitate virtual simulations, allowing for highly accurate predictions of the patient's postoperative head shape. The integration of suture biology knowledge with modern computational modeling currently forms the foundation for the safe and effective treatment of craniosynostosis [4-8].

In 2008, stainless steel spring-like distractors were introduced at Great Ormond Street Hospital for Children (GOSH – London, UK) to support posterior vault expansion – spring assisted posterior vault expansion (SAPVE) – in patients affected by SC [9, 10].

The primary research trends in this field focus on developing precise physico-mechanical and material models to facilitate a profound understanding of natural processes, such as postnatal craniofacial growth. Utilizing advanced imaging data, specialists can develop anatomical models perfectly tailored to the individual patient or the specific characteristics of a given population. These technologies find comprehensive application in planning highly complex procedures, including advanced reconstructive cranial surgery. Biomechanical simulations allow clinicians to precisely predict postoperative tissue alignment and final anatomical shape. Integrating innovative measurement techniques into daily clinical practice directly translates to enhanced preparation for the medical team, minimization of complication risks, and a significant increase in patient safety. Ultimately, interdisciplinary collaboration between engineers and clinicians facilitates the continuous refinement of medical procedures in the most demanding fields of modern surgery [11-14].

The aim of the study was a numerical analysis of biomechanical discrepancies occurring during the simulation of spring-assisted distraction. The analysis was conducted on three-dimensional skull models of infants aged 3, 6, and 12 months, which were generated based on computed tomography data. After processing the surface meshes in the Geomagic Design X and MeshMixer software, the models were subjected to virtual surgical planning with a designated osteotomy width of 16 mm. The placement of distraction springs was investigated according to the scheme from the KLS Martin catalog, i.e., at a distance of 25 mm from the coronal suture and 55 mm from the lambdoid suture. In the ANSYS environment, loads from springs with forces of 4.8 N, 8 N, and 13.2 N were simulated, taking into account a physiological intracranial pressure of 2666.4 Pa, which continuously stimulates the outward displacement of the released bone flaps.

2. Materials and methods

The basis for developing the numerical model was a CT scan of a child's skull with congenital craniosynostosis. The shape of the skull, unnaturally elongated in the anterior-posterior axis, along with flattened sides, suggests scaphocephaly. The physical dimensions of the model are: width 105 mm, length 159 mm, and height 158 mm. The cephalic index in this case is approximately 66, which is typical for a hyperdolichocephalic skull (Fig. 1). As part of the Virtual Surgical Planning (VSP), long surgical cuts (osteotomies) along the cranial vault were planned. Their purpose is to "release" the fused bones, which, combined with appropriate distraction springs, will allow the child's growing brain to expand the skull laterally [15-17].

The model includes burr holes that facilitate the safe separation of the bones from the meninges during surgery. From a biomechanical perspective, the optimal time to perform the procedure is before the age of 1, before the bones become harder and lose their plasticity, which could significantly complicate the remodeling process.

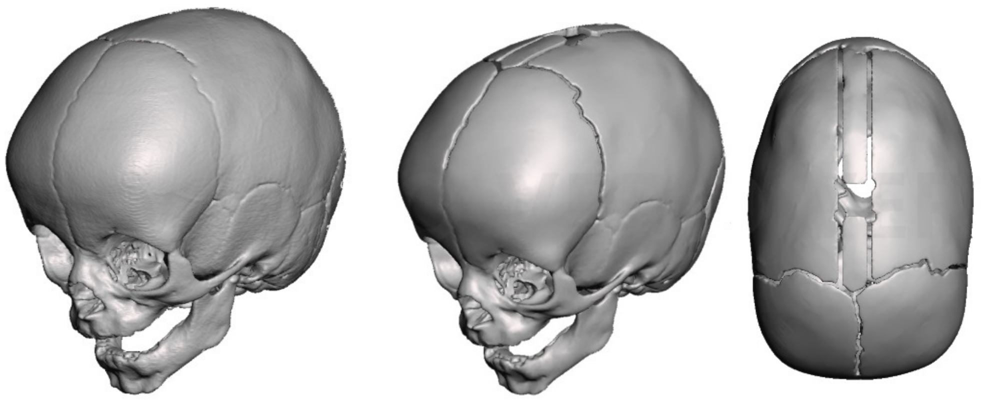

Fig. 1. Head CT of a child with congenital craniosynostosis and a skull model of a child with scaphocephaly, with planned surgical cuts

3. Computational assumptions and configuration of spring-assisted distraction in ANSYS

Three-dimensional skull models of infants aged 3 months, 6 months, and 12 months with sagittal craniosynostosis were developed. The thickness of the parietal bones in the constructed model varies from 1.5 mm to 3.5 mm. The osteotomy width was 16 mm. The action of two distraction springs was simulated according to the scheme from the KLS Martin catalog "CranioXpand Cranial springs for the treatment of sagittal craniosynostoses" [18]; the springs are placed at a distance of 25 mm from the coronal suture and 55 mm from the lambdoid suture. The effects of forces (Fig. 2) amounting to 4.8 N, 8 N, and 13.2 N, originating respectively from KLS Martin springs with diameters of 1 mm, 1.2 mm, and 1.6 mm, were numerically simulated.

$$[K]\{U\} = \{F_{ext}\} \tag{1}$$

$[K]$ is the global stiffness matrix of the system (dependent on the Young's modulus of infant bones and sutures), $\{U\}$ is the vector of nodal displacements, and $\{F_{ext}\}$ is the vector of external loads, which includes distributed forces from the springs and physiological intracranial pressure. The expanding forces were not applied at single points (which could generate artificial stress singularities) but as vector loads distributed over defined contact surfaces (approx. 2 mm^2 each), which accurately simulates the actual contact of the distractor footplates with the bone tissue. Boundary conditions included the removal of six degrees of freedom (Fixed Support) in the skull base area (mirroring the natural support on the spine) and at single points in the region of the sagittal suture to stabilize the model.

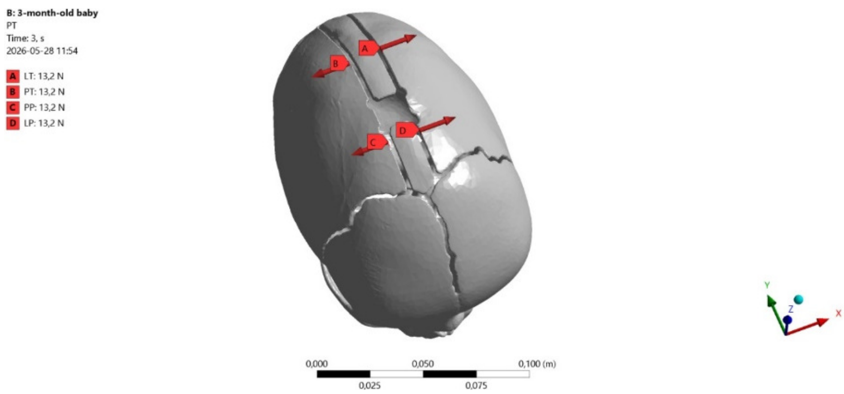

Fig. 2. Layout diagram of the distraction springs

A slow compression (correction of craniosynostosis-type defects) was simulated in the analysis. The loads are quasi-static in nature (slow, without dynamic or wave effects), thus the definition of material properties can be performed using a linear elastic model.

$$\sigma_{ij} = \frac{E}{1+\nu}\varepsilon_{ij} + \frac{E\nu}{(1+\nu)(1-2\nu)}\varepsilon_{kk}\,\delta_{ij} \tag{2}$$

Where σ_{ij} is the stress tensor, ε_{ij} is the small strain tensor, E is the Young's modulus (whose values are presented in Table 1), ν is the Poisson's ratio, and δ_{ij} is the Kronecker delta.

During the first year of a child's life, the skull undergoes radical changes. A discrepancy exists in the biomechanical literature: some researchers indicate a rapid increase in the Young's modulus (E) with age, while others (e.g., Coats and Margulies [16] and Baumer et al. [17]) have shown that the stiffness of the bone material itself does not change drastically in the first year of life. They proved that the increase in skull resistance is mainly due to increasing bone thickness and suture ossification. In this study, the latter approach was considered more reliable in the context of slow spring-assisted distraction, as it better reflects the compliance of young tissue to long-term, quasi-static loading. Based on data available in the literature (specifically bending and tensile tests described by McPherson and Kriewall [19] and Li et al. [20]), as well as the authors' own clinical and engineering experience, the skull bone material was defined as isotropic and linear elastic. Averaged stiffness values were adopted, providing a safe and logical gradient for numerical simulations in the age range of 3 to 12 months (Table 1). This approach optimizes computation time while maintaining high consistency with the actual biological response of infant tissues to slow deformations.

Table 1. Material properties of a child's skull bones

Child's age	Young's modulus (E) [MPa]	Poisson's ratio (ν)	Density (ρ) [kg/m^3]
3 months	350	0.28	1500
6 months	700	0.28	1600
12 months	1400	0.25	1700

Determining the material properties of cranial sutures in infants depends on how we define the examined area. There are two main approaches to this issue in biomechanics: modeling pure fibrous tissue and a macroscopic approach to the entire joint (taking into account progressive ossification). To apply this macroscopic approach in FEM analyses, equivalent numerical properties must be determined. In the latest computational models (e.g., simulating skull development and craniosynostosis), the suture is not treated as a constant material but as a dynamically changing transition zone. Progressive marginal mineralization and bone interdigitation are taken into consideration. In such macroscopic models, the "effective" substitute elasticity modulus (bulk modulus) increases stepwise with age, starting from approximately 30 MPa at birth, reaching about 90 MPa for a 3-month-old child, increasing to 150 MPa for a 6-month-old, and estimated at 230 MPa - 250 MPa for a 12-month-old.

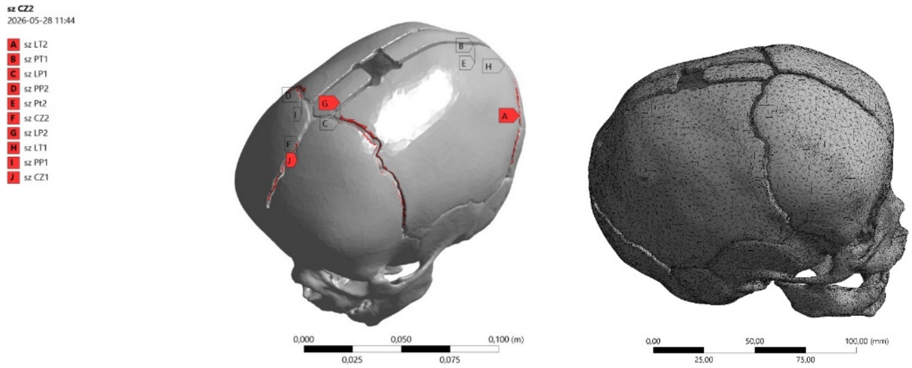

Fig. 3. Diagram of cranial suture arrangement in the model, view with the mesh applied in the ANSYS program

A contact was implemented to simulate the macroscopic stiffening of the entire joint (resulting from the closure of the suture and the interdigitation of bones). In ANSYS, this was achieved by assigning the so-called Absolute Normal Stiffness to the contacts. To convert Young's modulus to contact stiffness in ANSYS, the following computational formulas were used:

$$K_n = \frac{E_{eff}}{w} \tag{3}$$

$$F_{contact} = k_n \, \delta_n \tag{4}$$

where K_n is the normal contact stiffness (Penalty Stiffness), E_{eff} is the effective Young's modulus of the joint, w is the initial width of the suture gap, and δ_n is the penetration at the interface.

For this specific skull model, with irregular bone edges and clear gaps, an approach based on Bonded contacts with defined absolute stiffness (Pure Penalty) is the most appropriate method. Since the edges do not meet perfectly, the contact will act as an elastic layer of "glue" with a thickness equal to the gap. The stiffness of this joint in ANSYS (expressed in N/mm^3) is defined as the ratio of the effective Young's modulus of the joint to the average width of the suture (here we assume an average of 2 mm based on typical anatomy for the presented geometric model). The calculated values of Normal Stiffness of cranial sutures in infants for individual cases are as follows for children aged: 3 months: 45 N/mm^3 (the most compliant skull, allows for the greatest "opening" of sutures under load), 6 months: 75 N/mm^3 (moderate stiffening resulting from the beginning of bone edge interdigitation), 12 months: 120 N/mm^3 (the stiffest joint, simulating a narrow, strongly interdigitated suture with the beginnings of mineralization) [21-23].

The finite element mesh was generated in the ANSYS Meshing module. Tetrahedral elements (ten-node, quadratic shape functions) were used in the analysis, which enable precise mapping of complex geometry shapes. The total number of elements was 567,232, and the number of nodes was 985,292. In order to verify the correctness of the numerical model and rule out the influence of discretization on the obtained results, a mesh convergence analysis was performed. The study aimed to confirm that the adopted finite element mesh density allows for obtaining reliable results of displacements and stresses in the analyzed full skull model, independent of the division. Two FEM mesh variants were built and analyzed for identical geometry of the complete skull (including the neurocranium, viscerocranium, and mandible). In both cases, tetrahedral elements were used, and mesh refinement control was executed through a global change of element size using the Body Sizing function. Identical boundary conditions and loads were applied to both discrete models within the static analysis. Bilateral compression on the skull bones was modeled using two concentrated forces of 15 N each, while maintaining the same geometry fixation locations. The conducted analysis demonstrates that the numerical model is stable. Refining the mesh by reducing the element size from 5 mm to 3 mm yields minimal differences in global stiffness (displacement changes on the order of 2 %) and results in predictable, localized stress map variations. Based on the obtained results, it can be concluded that the base mesh with a 5 mm element size ensures sufficient convergence of results, and its use is justified due to the optimization of computation time while maintaining high simulation reliability.

4. Results

The selection of an appropriate failure criterion for infant bones is crucial because they behave completely differently than adult bones. The calvarial bone in children during their first year of life is much more elastic, compliant to deformations, and less mineralized. Instead of undergoing brittle fracture, it often succumbs to plastic indentation (so-called "greenstick" or depressed fractures). For this reason, in pediatric biomechanics, there is a shift away from the Huber-Mises-Hencky (Von Mises) criterion, standard for steel, towards criteria that better describe the fracturing of biological materials under force loading.

The eigenvalues of the stress tensor (principal stresses σ_1, σ_2, σ_3) are obtained by solving the characteristic equation:

$$\det\left(\sigma_{ij} - \lambda\delta_{ij}\right) = 0 \tag{5}$$

The principal strains ε_1 are determined analogously. It was assumed that the initiation of fracture or permanent deformation of bone tissue in infants occurs when the maximum principal tensile strain exceeds the permissible limit value:

$$(\varepsilon_1 \geq \varepsilon_{crit}) \tag{6}$$

defined in Table 2.

The best criteria to apply in a numerical simulation are:

- Maximum Principal Strain: In the case of very young and elastic bones, it is not the force (stress) itself, but the limit stretching of the fibers that determines the fracture. The bone fractures when it is stretched too much, typically on the outer side relative to the bending site. This best reflects the failure mechanics of infant bone, which can withstand large stresses through significant deformation.
- Maximum Principal Stress: This criterion assumes that the material will fail when the highest tensile stress exceeds the tensile strength limit of the bone. Bones are generally much weaker in tension than in compression. This allows for the precise localization of the crack initiation site (linear skull fracture), which usually starts in the zone of highest tension.

Because an isotropic and linear elastic material was assumed in the model, exceeding the following values (based, among others, on the works of Coats and Margulies) represents the point in the numerical simulation where bone fracture or its permanent deformation would actually occur. With age, the bone becomes stronger (withstands greater stresses) but at the same time more brittle (fractures at smaller strains) [19, 20].

Table 2. Limit values beyond which bone damage (fracture or permanent plastic deformation) occurs

Child’s age	Limit Principal Stress [MPa]	Limit Principal Strain [–]
3 months	10-14	0.08-0.12 (8 % - 12 %)
6 months	15-20	0.06-0.09 (6 % - 9 %)
12 months	22-30	0.04-0.07 (4 % - 7 %)

4.1. Summary of obtained numerical test results for a 3-month-old child’s skull

The screenshots presented below (Figs. 4-6) show the distribution of Maximum Principal Strain (Table 3) in the 3-month-old child’s skull model subjected to spring--assisted distraction. This analysis allows researchers to evaluate the biomechanical reaction of bone tissue to expanding forces, which is crucial for predicting the stimulation of bone growth in the osteotomy gaps.

Table 3. Maximum Principal Strain

	Minimum [mm/mm]	Maximum [mm/mm]	Average [mm/mm]
4.8 N	–0.00007	0.15503	0.00083
8 N	–0.00010	0.20701	0.00110
13.2 N	–0.00014	0.28948	0.00151

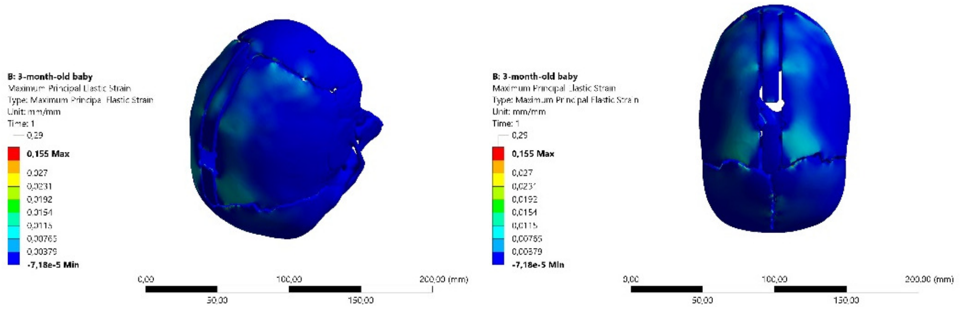

Fig. 4. Distribution of Maximum Principal Strain in the 3-month-old infant skull model in isometric and top views. Numerical analysis results for a spring distraction force of 4.8 N

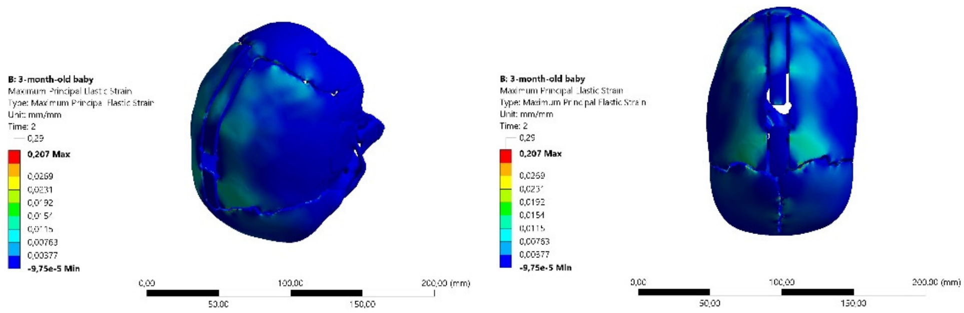

Fig. 5. Distribution of Maximum Principal Strain in the 3-month-old infant skull model in isometric and top views. Numerical analysis results for a spring distraction force of 8 N

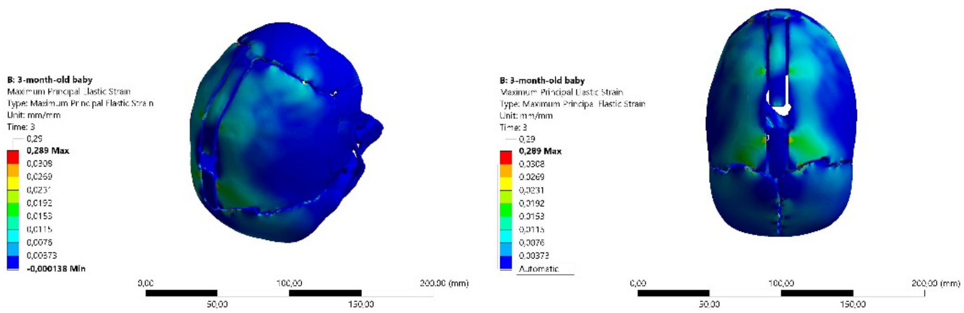

Fig. 6. Distribution of Maximum Principal Strain in the 3-month-old infant skull model in isometric and top views. Numerical analysis results for a spring distraction force of 13.2 N

The screenshots presented below (Figs. 7-9) show the distribution of Maximum Principal Stress (Table 4) in the 3-month-old child's skull model subjected to spring--assisted distraction.

Table 4. Maximum Principal Stress

	Minimum [MPa]	Maximum [MPa]	Average [MPa]
4.8 N	–8.263	40.530	0.240
8 N	–10.884	55.794	0.318
13.2 N	–14.854	82.592	0.435

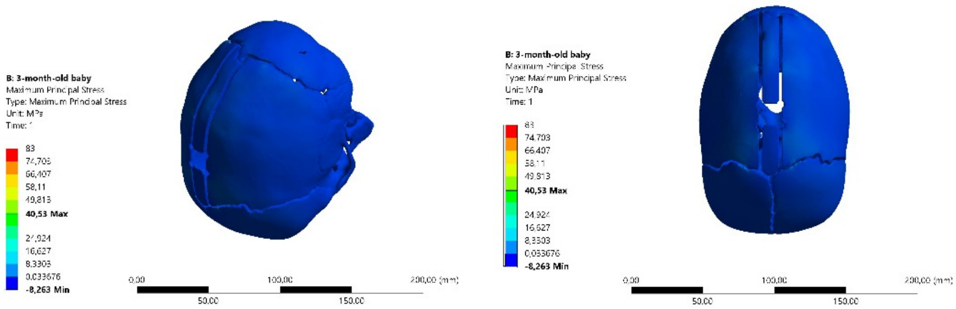

Fig. 7. Distribution of Maximum Principal Stress in the 3-month-old infant skull model in isometric and top views. Numerical analysis results for a spring distraction force of 4.8 N

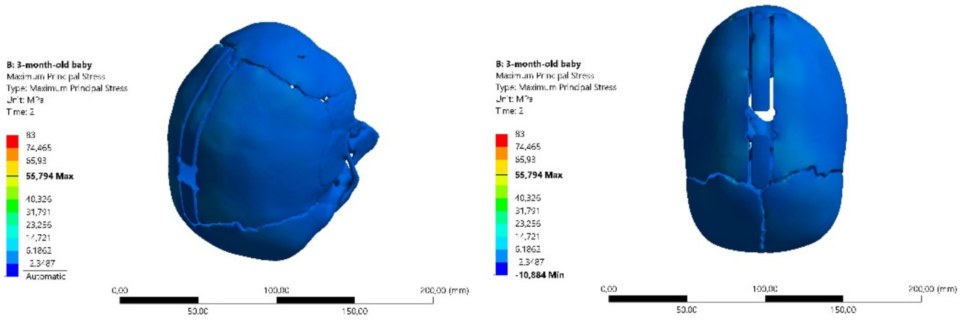

Fig. 8. Distribution of Maximum Principal Stress in the 3-month-old infant skull model in isometric and top views. Numerical analysis results for a spring distraction force of 8 N

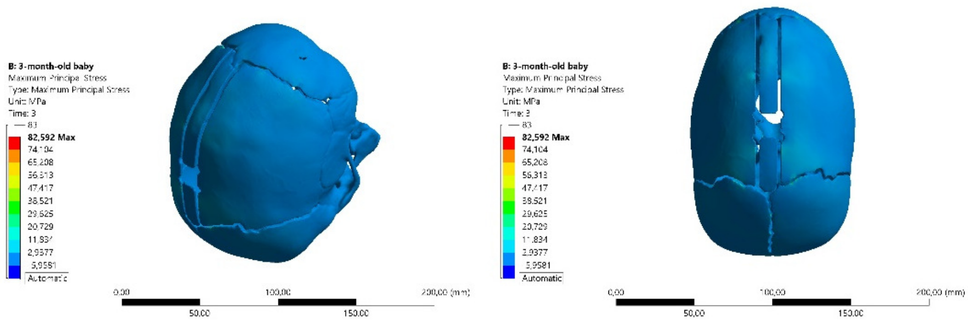

Fig. 9. Distribution of Maximum Principal Stress in the 3-month-old infant skull model in isometric and top views. Numerical analysis results for a spring distraction force of 13.2 N

4.2. Summary of obtained numerical test results for a 6-month-old child's skull

The screenshots presented below (Figs. 10-12) show the distribution of Maximum Principal Strain (Table 5) in the 6-month-old child's skull model subjected to spring-assisted distraction. This analysis allows evaluating the biomechanical reaction of bone tissue to expanding forces, which is crucial for predicting the stimulation of bone growth in the osteotomy gaps.

Table 5. Maximum Principal Strain

	Minimum [mm/mm]	Maximum [mm/mm]	Average [mm/mm]
4.8 N	–0.00006	0.07236	0.00043
8 N	–0.00005	0.09784	0.00058
13.2 N	–0.00007	0.14070	0.00083

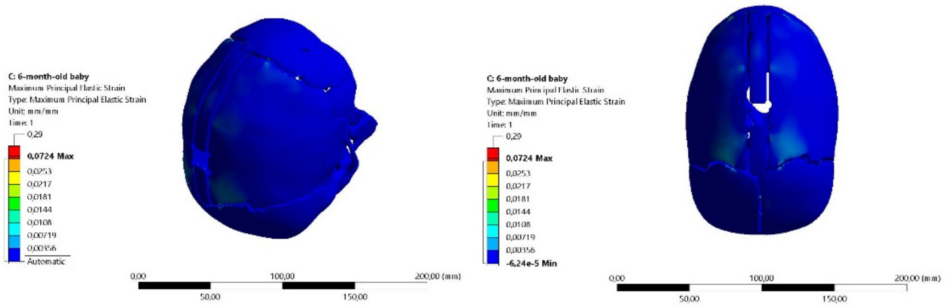

Fig. 10. Distribution of Maximum Principal Strain in the 6-month-old infant skull model in isometric and top views. Numerical analysis results for a spring distraction force of 4.8 N

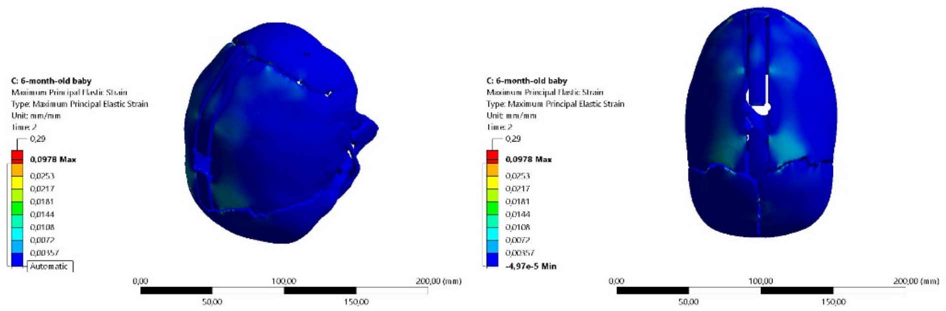

Fig. 11. Distribution of Maximum Principal Strain in the 6-month-old infant skull model in isometric and top views. Numerical analysis results for a spring distraction force of 8 N

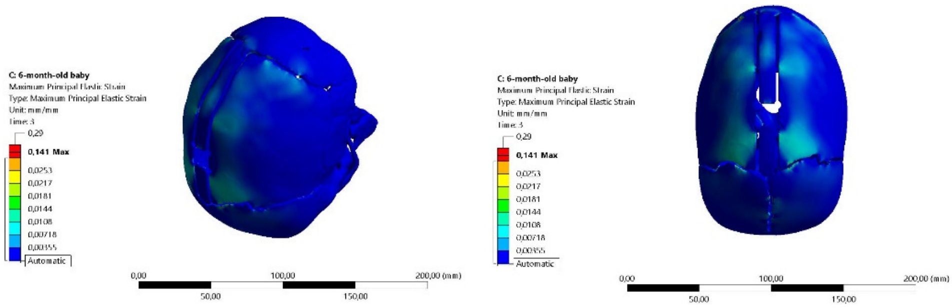

Fig. 12. Distribution of Maximum Principal Strain in the 6-month-old infant skull model in isometric and top views. Numerical analysis results for a spring distraction force of 13.2 N

The screenshots presented below (Figs. 13-15) show the distribution of Maximum Principal Stress (Table 6) in the 6-month-old child's skull model subjected to spring-assisted distraction.

Table 6. Maximum Principal Stress

	Minimum [MPa]	Maximum [MPa]	Average [MPa]
4.8 N	–8.249	37.425	0.250
8 N	–10.990	52.556	0.336
13.2 N	–15.418	78.759	0.473

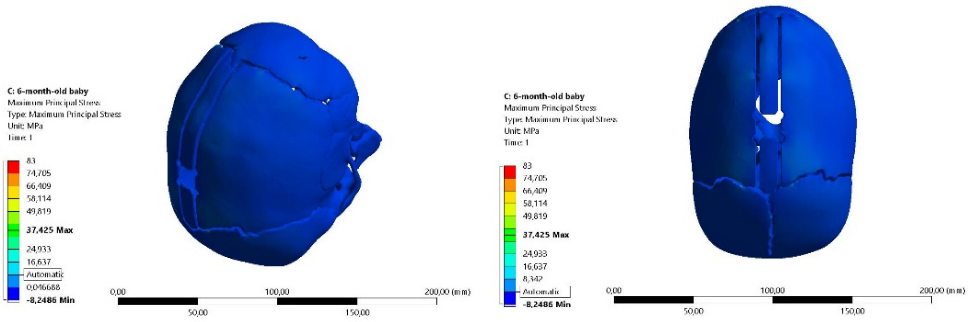

Fig. 13. Distribution of Maximum Principal Stress in the 6-month-old infant skull model in isometric and top views. Numerical analysis results for a spring distraction force of 4.8 N

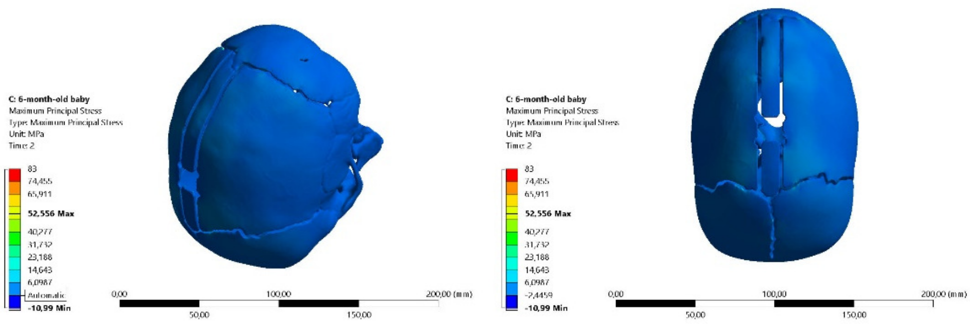

Fig. 14. Distribution of Maximum Principal Stress in the 6-month-old infant skull model in isometric and top views. Numerical analysis results for a spring distraction force of 8 N

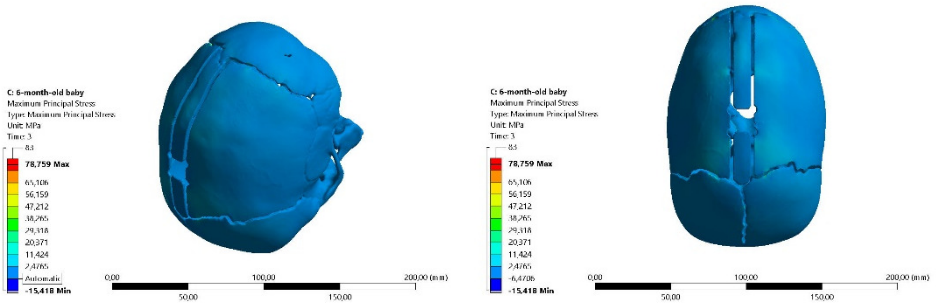

Fig. 15. Distribution of Maximum Principal Stress in the 6-month-old infant skull model in isometric and top views. Numerical analysis results for a spring distraction force of 13.2 N

4.3. Summary of obtained numerical test results for a 12-month-old child's skull

The screenshots presented below (Figs. 16-18) show the distribution of Maximum Principal Strain (Table 7) in the 12-month-old child's skull model subjected to spring-assisted distraction. This analysis allows evaluating the biomechanical reaction of bone tissue to expanding forces, which is crucial for predicting the stimulation of bone growth in the osteotomy gaps.

Table 7. Maximum Principal Strain

	Minimum [mm/mm]	Maximum [mm/mm]	Average [mm/mm]
4.8 N	–0.00003	0.03319	0.00022
8 N	–0.00004	0.04465	0.00029
13.2 N	–0.00005	0.06408	0.00042

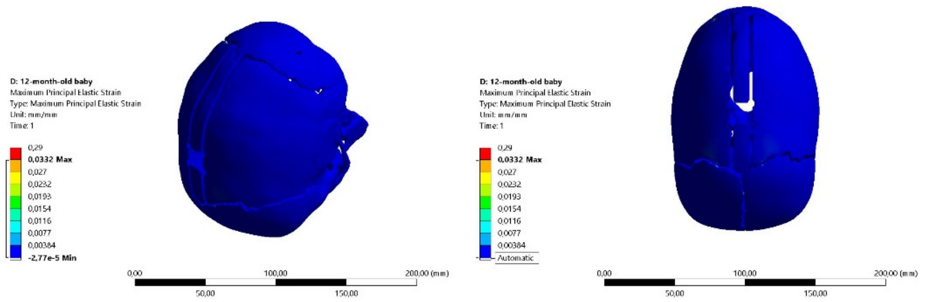

Fig. 16. Distribution of Maximum Principal Strain in the 12-month-old infant skull model in isometric and top views. Numerical analysis results for a spring distraction force of 4.8 N

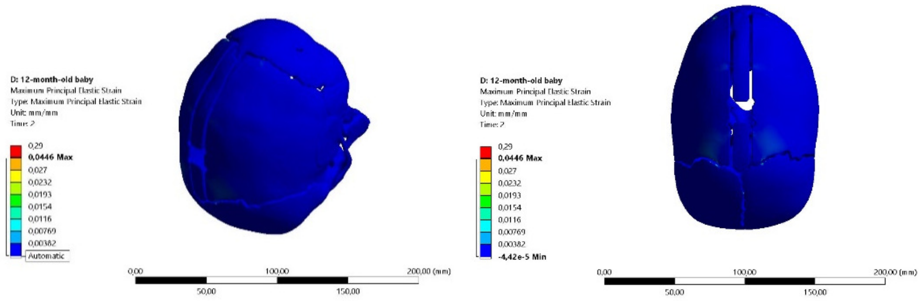

Fig. 17. Distribution of Maximum Principal Strain in the 12-month-old infant skull model in isometric and top views. Numerical analysis results for a spring distraction force of 8 N

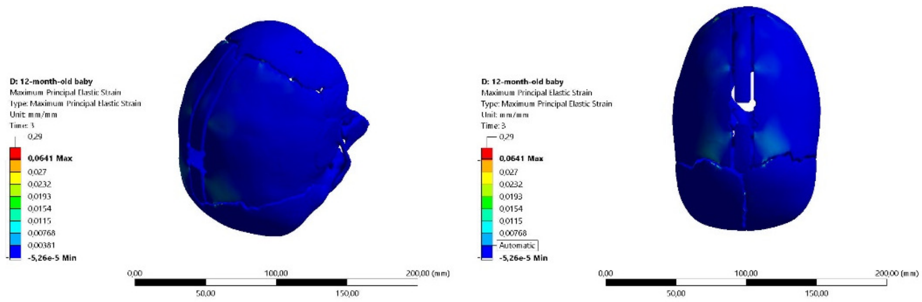

Fig. 18. Distribution of Maximum Principal Strain in the 12-month-old infant skull model in isometric and top views. Numerical analysis results for a spring distraction force of 13.2 N

The screenshots presented below (Figs. 19-21) show the distribution of Maximum Principal Stress (Table 8) in the 12-month-old child's skull model subjected to spring-assisted distraction.

Table 8. Maximum Principal Stress

	Minimum [MPa]	Maximum [MPa]	Average [MPa]
4.8 N	–6.752	36.914	0.254
8 N	–8.998	49.672	0.342
13.2 N	–12.691	76.651	0.486

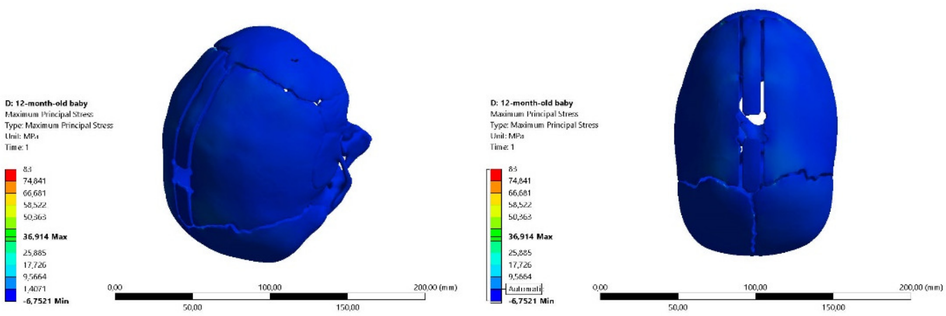

Fig. 19. Distribution of Maximum Principal Stress in the 12-month-old infant skull model in isometric and top views. Numerical analysis results for a spring distraction force of 4.8 N

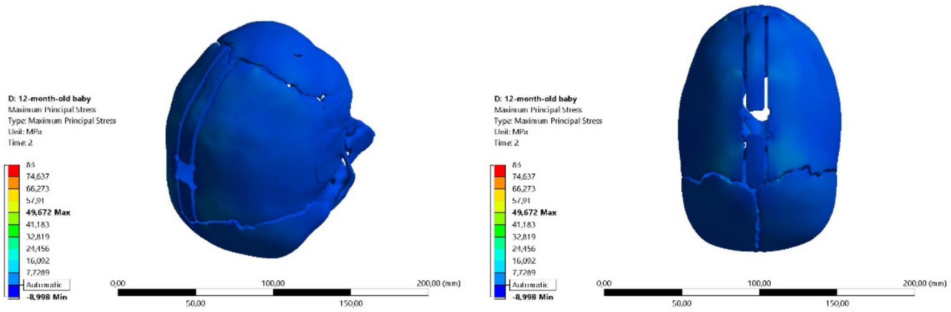

Fig. 20. Distribution of Maximum Principal Stress in the 12-month-old infant skull model in isometric and top views. Numerical analysis results for a spring distraction force of 8 N

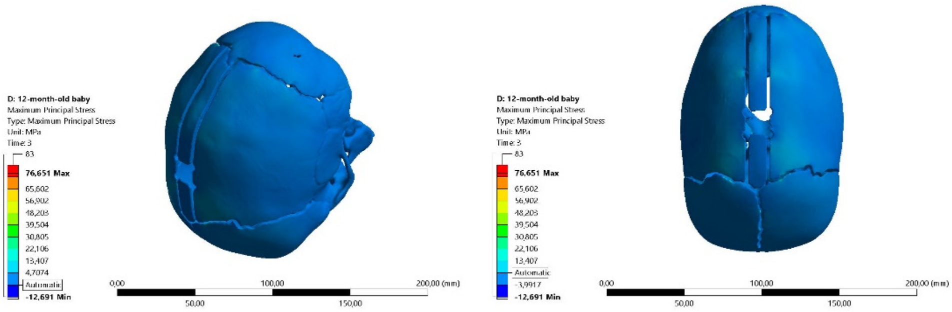

Fig. 21. Distribution of Maximum Principal Stress in the 12-month-old infant skull model in isometric and top views. Numerical analysis results for a spring distraction force of 13.2 N

5. Conclusions

In a 3-month-old child, the skull is most susceptible to deformation, and the permissible principal strain is the highest (8 % - 12 %). Maximum strains range from approx. 15.5 % for a force of 4.8 N to as much as 28.9 % for a force of 13.2 N. All three loading cases significantly exceed the permissible limits. The maximum principal stresses fall within the range of 40.53 MPa to 82.59 MPa. These values drastically exceed the 10 MPa - 14 MPa limit. The application of the tested forces (from 4.8 N to 13.2 N) in the established scheme for a 3-month-old child will highly likely lead to local destruction of bone tissue. The total deformation here reaches from 8.9 mm to over 15 mm, which indicates a very significant interference into the structure of the soft skull.

In a 6-month-old child, the skull begins to stiffen, and the limit of permissible strain decreases (6 % - 9 %), while the tensile strength slightly increases (15 MPa - - 20 MPa). Strains for the lowest force of 4.8 N – the maximum strain is approx. 7.2 %, which falls within the safe limit of 6 % - 9 %. However, for forces of 8 N (approx. 9.7 %) and 13.2 N (approx. 14 %), the strains once again exceed the failure criterion. Maximum stresses range from 37.42 MPa to 78.75 MPa. Although the bone is stronger than at 3 months of age, these stresses still significantly exceed the 15 MPa - - 20 MPa limit, suggesting localized overloading. A force of 4.8 N appears to be on the verge of safety in terms of strains, however, higher forces still generate excessive loads. Total displacements are much smaller than in a 3-month-old child (from 4.9 mm to 9.1 mm).

In a 12-month-old child, the skull is the stiffest (fusing sutures, thicker bone), which results in a higher tensile strength (22 MPa - 30 MPa) but the lowest tolerance for deformation (4 % - 7 %). Maximum strains are the lowest here: approx. 3.3 % for a force of 4.8 N; 4.4 % for 8 N; and 6.4 % for 13.2 N. All these values fall within the safe range or at its limit (the limit is 4 % - 7 %). Despite safe strain levels, maximum stresses still reach quite high values (from 36.91 MPa for 4.8 N to 76.65 MPa for 13.2 N). The permissible limit of 22 MPa - 30 MPa is exceeded. Due to the high stiffness of the skull at this age (total deformation is merely from 2.6 mm to 4.9 mm), the bone is not subjected to excessive stretching, therefore the principal strain criterion does not signal failure. However, high stresses and high reduced von Mises stresses (up to 129.2 MPa) may indicate the occurrence of very high, localized force concentrations directly at the points of contact between the springs and the bone.

The highest stresses and strains concentrate at the poles of the gaps (at the ends of the bone cuts). This is a typical phenomenon from the point of view of mechanics (notch effect), where the apex of the cut accumulates stress. Additionally, a clear load is visible in the region of the skull base and the coronal/lambdoid sutures, which indicates that the force from the springs is transferred to neighboring anatomical structures. In addition to the cutting sites themselves (osteotomies), the analysis indicates a transfer of strains to other cranial sutures that are not yet ossifying at this age. This indicates that skull modeling using springs influences a global change in its shape, and not just the localized widening of the gap.

The authors propose a solution involving a wider spacing of the distraction springs, which results in different skull shaping than in the case of springs positioned according to the manufacturer's guidelines. The allocation of springs and the distraction force should be tailored to the skull shape in such a way as to account for the highly complex and often pathologically altered bone structure. Based on the numerical studies conducted, it was also found that craniosynostosis treatment planning can be designed in such a way as to introduce a personalized force into areas that are critical from the perspective of shaping the skull bones. This allows for unloading areas with bone defects or complex tissue anomalies while increasing loads in areas where the bone needs to be displaced to achieve the planned clinical outcome.

The Team's future research planning focuses on assessing the magnitude and nature of bone loading criteria across various allocations along the cut line, utilizing different configurations of distraction springs. The current state of the art does not allow the use of springs with a personalized, highly precisely selected distraction force. This presents another design and technological challenge that could significantly improve the treatment process for children with this severe congenital disease.

References

[1] Harrison, L.M., Edison R.L., & Hallac, R.R. (2025). Artificial intelligence applications in pediatric craniofacial surgery. *Diagnostics*, *15*(7), 829. DOI: 10.3390/diagnostics15070829.

[2] Keishing, V., Ahn, E.S., Khasim, Z., Loudermilk, A.D., & Ericson, B.J. (2025). Towards automated craniosynostosis diagnosis using efficientNet-based artificial intelligence models: A two--class and multi-class approach. *Journal of Imaging Informatics in Medicine*, 284716473. DOI: 0.1007/s10278-025-01694-1.

[3] Guo, Y., Keeme-Sayre, A.G., Mudie, L.I., Williams, K.J., & Yen, M.T. (2025). Resorbable versus nonresorbable implants in pediatric orbital fracture repair. *Journal of Craniofacial Surgery*, *1*, 37(6), 1466-1468. DOI: 10.1097/SCS.0000000000012224.

[4] Opperman, L.A. (2000). Cranial sutures as intramembranous bone growth sites. *Developmental Dynamics*, *219*, 472-485. DOI: 10.1002/1097-0177(2000)9999:9999%3c:AID-DVDY1073%3e3.0.CO;2-F.

[5] Fearon, J.A. (2014). Evidence-based medicine: craniosynostosis. *Plastic and Reconstructive Surgery*, *133*, 1261-1275. DOI: 10.1097/PRS.0000000000000093.

[6] Garza, R.M., & Khosla, R.K. (2012). Nonsyndromic craniosynostosis. *Seminars in Plastic Surgery*, *26*(2), 53-63. DOI: 10.1055/s-0032-1320063.

[7] Wall, S., Thomas, G., & Johnson, D. (2014). The preoperative incidence of raised intracranial pressure in nonsyndromic sagittal craniosynostosis is underestimated in the literature: clinical article. *Journal of Neurosurgery: Pediatrics*, *14*, 674-681.

[8] Heutinck, P., et al. (2021). Statistical shape modelling for the analysis of head shape variations. *Journal of Cranio-Maxillo-Facial Surgery*, *49*, 449-455. DOI: 10.1016/j.jcms.2021.02.020.

[9] Borghi, A., Rodriguez-Florez, N., Ruggiero, F., James, G., O'Hara, J., Ong, J., & Schievano, S. (2019). A population-specific material model for sagittal craniosynostosis to predict surgical shape outcomes. *Biomechanics and Modeling in Mechanobiology*, *19*, 1-11. DOI: 10.1007/s10237-019-01229-y.

[10] Borghi, A., Rodriguez-Florez, N., Rodgers, W., James, G., Hayward, R., Dunaway, D., & Schievano, S. (2018). Spring assisted cranioplasty: a patient specific computational model. *Medical Engineering & Physics*, *53*, 58-66. DOI: 10.1016/j.medengphy.2018.01.001.

[11] Breakey, W., Knoops, P.G.M., Borghi, A., Rodriguez-Florez, N., Dunaway, D.J., Schievano, S., & Jeelani, O.N.U. (2017). Intracranial volume measurement: a systematic review and comparison of different techniques. *Journal of Craniofacial Surgery*, *28*(7), 1746-1751. DOI: 10.1097/SCS.0000000000003929.

[12] Breakey, R.W.F., Knoops, P.G., Borghi, A., Rodriguez-Florez, N., O'Hara, J., James, G., & Jeelani, N.O. (2018). Intracranial volume and head circumference in children with unoperated syndromic craniosynostosis. *Plastic and Reconstructive Surgery*, *142*(5), 708-717. DOI: 10.1097/PRS.0000000000007147.

[13] Zhang, F., Kanik, J., Mansi, T., et al. (2017). Towards patient-specific modeling of mitral valve repair: 3D transesophageal echocardiography-derived parameter estimation. *Medical Image Analysis*, *35*, 599-609. DOI: 10.1016/j.media.2016.09.006.

[14] Liang, C., Marghoub, A., Profico, A., Costantino Buzi, C., Didziokas, M., Van de Lande, L., Khonsari, R.H., Johnson, D., O'Higgins, P., & Moazen, M. (2024). A physico-mechanical model of postnatal craniofacial growth in human. *iScience*, *29*, 27(9), 110617. DOI: 10.1016/j.isci.2024.110617.

[15] Couper, Z.S., & Albermani, F.G. (2025). Biomechanics of shaken baby syndrome: physical testing and numerical modeling. In *Developments in Mechanics of Structures and Materials*, Vol. 1, Deeks & Hao (eds). London: Taylor & Francis Group.

[16] Coats, B., & Margulies, S.S. (2006). Material properties of human infant skull and suture at high rates. *Journal of Neurotrauma*, *23*(8), 1222-1232. DOI: 10.1089/neu.2006.23.1222.

[17] Baumer, T.G., Powell, B J., Fenton, T.W., & Haut, R.C. (2009). Age dependent mechanical properties of the infant porcine parietal bone and correlation with human. *Journal of Biomechanical Engineering*, *131*(11), 111-116.

[18] KLS Martin Group. CranioXpand Cranial springs for the treatment of sagittal craniosynostoses.

[19] Alawadhi, E.M. (2015). *Finite Element Simulations Using ANSYS*. Palm Bay: Apple Academic Press Inc. DOI: 10.1201/b18949.

[20] Chen, X., & Liu, Y. (2018). *Finite Element Modeling and Simulation with ANSYS Workbench*. Boca Raton: CRC Press.

[21] Lee, H.H. (2025). *Finite Element Simulations with ANSYS Workbench 2023*. Mission: SDC Publications: Mission. DOI: 10.1201/9781351045872.

[22] McPherson, G.K., & Kriewall, T.J. (1980). The elastic modulus of fetal cranial bone: a first step towards an understanding of the biomechanics of fetal head molding. *Journal of Biomechanics*, *13*(1), 9-16.

[23] Li, Z., Hu, J., Reed, M.P., et al. (2011). Development, validation, and application of a parametric pediatric head finite element model for impact simulations. *Annals of Biomedical Engineering*, *39*, 2984-2997.